Partial-Reference Sonar Image Quality Assessment for Underwater Transmission

WEILING CHEN
Key Laboratory of Underwater Acoustic Communication and Marine Information Technology, Ministry of Education, Xiamen University, China

KE GU
BJUT Faculty of Information Technology, Beijing University of Technol1ogy, Beijing, China

XIONGKUO MIN
Shanghai Jiaotong University, Shanghai, China

FEI YUAN
EN CHENG
Key Laboratory of Underwater Acoustic Communication and Marine Information Technology, Ministry of Education, Xiamen University, China

WENJUN ZHANG, Fellow, IEEE
Shanghai Jiaotong University, Shanghai, China

The rapid growth of ocean exploration has led to an increase in the demand of sonar images, since they contain a great amount of information collected by sonar systems such as distributions of underwater creatures and minerals. For further analysis, sonar images usually need to be transmitted via underwater acoustic channel (UAC). However, the hostile nature of UAC makes the transmitted sonar images have high probability to be afflicted with distortions introduced in transmission procedures. To monitor image quality, a partial-reference sonar image quality predictor (PSIQP) is proposed in this paper. A unique property that differentiates the proposed PSIQP metric from existing works is the consideration of the viewing behavior of the human visual system for sonar images, which motivates us to take both image perception and understanding into consideration. The results of experiments based on sonar image quality database show that the proposed metric provides accurate predictions across a variety of compression and transmission distortions.

Manuscript received July 11, 2017; revised February 20, 2018; released for publication February 22, 2018. Date of publication April 23, 2018; date of current version December 5, 2018.

DOI. No. 10.1109/TAES.2018.2829378

Refereeing of this contribution was handled by L. M. Kaplan.

This work was supported in part by the National Natural Science Foundation of China under Grant 61571377, Grant 61471308, Grant 61771412, and Grant 61703009 and in part by the Fundamental Research Funds for the Central Universities (20720180068).

Authors' addresses: W. Chen, F. Yuan, and E. Cheng are with the Key Laboratory of Underwater Acoustic Communication and Marine Information Technology, Ministry of Education, Xiamen University, Xiamen 361005, China, E-mail: (weiling.chen@stu.xmu.edu.cn; yuanfei@xmu.edu.cn; chengen@xmu.edu.cn); K. Gu is with the Beijing Key Laboratory of Computational Intelligence and Intelligent System, BJUT Faculty of Information Technology, Beijing University of Technology, Beijing 100124, China, E-mail: (guke.doctor@gmail.com); X. Min and W. Zhang are with Shanghai Jiaotong University, Shanghai 200030, China, E-mail: (minxiongkuo@gmail.com; zhangwenjun@sjtu.edu.cn). *(Corresponding author: En Cheng.)*

0018-9251 © 2018 IEEE

I. INTRODUCTION

Sonar can be used for hydrographic surveying and charting, sea life monitoring, and ocean rescue, etc. The quality of sonar image plays a crucial role in above-mentioned applications [1], [2], and it is necessary to send sonar images to a remote location for further analysis. Due to the poor condition of underwater acoustic channel (UAC), quality degradation is more easily to be introduced than in the terrestrial channel. The loss of information in transmission procedures (e.g., source compression coding and packet transmission) limits the visibility of the received images. Hence, sonar images transmitted via UAC are usually afflicted with noise, blur, structural degradation, and other distortions, and it is necessary to establish an effective objective quality assessment metric of sonar images.

There have been many categories of image quality assessment (IQA) methods when classified based on types of source images, including but not limited to IQA of nature scene images (NSIs) [3]–[5], screen content images (SCIs), [6], [7], stereoscopic images [8], [9], and medical images [10], etc. All these IQA methods were developed by considering the characteristics of relevant source images. For example, NSIs usually have rich color variations, complex texture content, and thick lines, which forming the pattern primarily for entertainment, while SCIs are mixed with NSIs and computer graphical content and full of uncomplicated shapes, limited color, and thin lines [11]. Stereoscopic images have higher dimensions, and medical images always reflect the scenes that can only be understood by experienced professionals. All these characteristics make existing IQA methods sort of ad-hoc for a specific type of image. Sonar images mostly have gray level, low contrast, and the structural information attracts more attention of viewers because sonar images are used for mapping and detecting instead of aesthetic appreciation in general. The characteristics and viewing behaviors of sonar images lead to the failure of existing IQA models to evaluate sonar image quality. So sonar IQA models need specially design according to their characteristics.

To tackle the problem of sonar IQA, the availability of reference needs consideration first. Most widely used IQA methods follow the full-reference (FR) approach due to its good performance. But there are some applications that are reference unavailable or are not entirely reference available, e.g., quality monitoring for image acquisition and transmission, etc. In those cases, reduced-reference (RR) methods [12]–[16] and no-reference (NR) methods [3], [6], [7] may be more appropriate. Current NR IQA methods usually do not perform well because they evaluate quality exclusively based on distorted signal and without any reference available, while RR IQA methods achieve better results than NR methods [17]. In the situation of

underwater acoustic transmission, a reference image would generally not be available at the receiver side, but partial information of original image can be transmitted to the receiver side as a reference via an ancillary channel or as an invisible and robust watermark embedded in transmitted image. Thus, the partial-reference sonar image quality predictor (PSIQP) is proposed in this paper.

Most existing quality evaluation algorithms aim to generate perceived quality scores, but subjective quality scores evaluated for sonar images considering the image utility as well [18]. Most sonar images are used for practical applications, for example, rescuing, underwater searching, underwater biological detection, and seabed mapping. In subjective quality assessment of sonar images, the evaluation will not be affected by any aesthetical element, but instead, image understanding is an important step in above-mentioned sonar image applications. Due to the essential role of image understanding for sonar image utilities [19] and the viewing behavior of the human visual system (HVS), the following factors will influence the quality of a sonar image.

1) The clarity of object contained in the image.
2) The amount of information can be extracted from the image.
3) The decrease of comfort due to quality degradation.

In accordance with these three factors, the PSIQP metric is designed with a three-stage framework. The first stage concerns the human perception of sonar images. It can be affected by the amount of information contained in a sonar image and the feeling of "comfort" provided by a sonar image. In this stage, too little useful information, too much useless information, or a drop of comfort due to the quality degradation will all lead to the decrease of perceived quality. The information and comfort indices will be extracted to reflect the quality perception of a sonar image. The second stage is influenced by image understanding that it is related to the effectiveness of sonar images. One of the essential approaches to understand a sonar image is to identify the object contained in it [20]. According to some research results in image processing, the structure plays a crucial role in object identification. Therefore, the structural similarity between the original and distorted sonar images is employed in this stage to represent the usefulness of a sonar image. Finally, the information and comfort indices and the structural similarity are systematically integrated for quality prediction in the third stage.

We arrange the reminder of this paper as follows. Section II describes the detail of our PSIQP metric explicitly. In Section III, performance comparisons of the PSIQP metric with selected existing RR and FR IQA methods are performed on the sonar image quality database (SIQD), which consists of sonar images and their distorted versions. We conclude this paper in Section IV.

II. PROPOSED PSIQP METRIC

A. RR-IQA-Based Underwater Transmission System

In many (if not all) applications, it is necessary to send images captured by sonar to a remote location for further analysis, which needs human decision because it is difficult to achieve automatic underwater target recognition according to the current state of the art. Compared to terrestrial channel, UAC presents a more constrained communication environment: More narrow bandwidth, longer transmission delay, larger and faster changed Doppler frequency shift and rapid fluctuation, etc [21]. Considering the limited channel bandwidth and large data amount of image, it is essential to apply efficient source coding for data compression. Since the importance of different parts in a bitstream after source coding is different in many cases [22], and there exists distortion concealment effect in the HVS [23], transmitted image quality evaluation based on quality of service indices such as bit error ratio have not always proved effective. As illustrated in Fig. 1, the occurrence of three bits errors in an important part of a compressed stream severely damages the image while three bits errors occurring in an unimportant part has little impact on image quality. Since the reference signal is not entirely available for underwater transmission, RR IQA plays a pivotal role in monitoring the quality of sonar image transmitted via UAC.

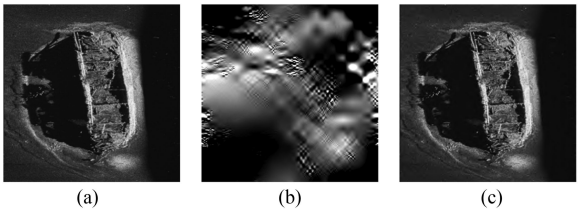

Fig. 1. Influence of three bits error occurred in bits with different importances. (a) Reference sonar image without bit error. (b) Three bits error in important part. (c) Three bits error in unimportant part.

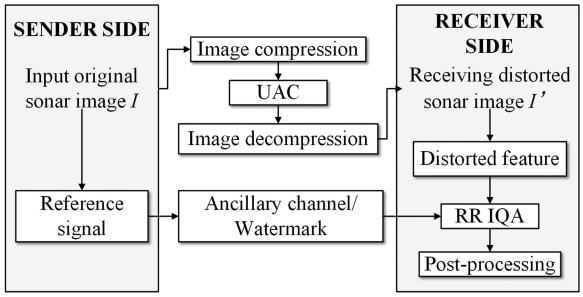

Fig. 2. Framework of a RR-IQA-based sonar image transmission system.

The first attempt of RR-IQA is proposed in [24] for monitoring the real-time video quality over wireless communication channel. Then, this philosophy is extended to different applications [12], [25]. For the underwater transmission system, RR IQA can serve as a guidance of post processing, e.g., retransmission, image restoration. The framework of a RR-IQA-based transmission system is depicted in Fig. 2. In the sender side, the reference signal of image captured by sonar will first be extracted. Then, the image is transmitted via UAC to a remote location for further analysis after being compressed. As for the reference signal, most existing works protect it by assuming an error-free ancillary channel with low data rate. In this paper, we consider an-

other viable option for reference signal transmission. There exists a kind of invisible watermarking strategy with high robustness, such kind of watermark is one viable alternative to ancillary channel for its ability of transmitting the reference signal alone with sonar image without being distorted. In receiver side, the feature extractor is applied to the received distorted image. The features extracted from the original and distorted sonar images are both employed in the sonar IQA. Finally, the post processing [26], [27] is conducted according to the result of RR sonar IQA. For RR sonar IQA, features should be selected considering the characteristics of the HVS and sonar images, and summary the quality of the whole image, such that the result of feature processing in receiver side can reflect the quality of sonar images and the post processing will be more effective.

B. Information and Comfort Indices

As mentioned earlier, the proposed PSIQP metric has a three-stage framework. The first stage considers image perception, which has no influence on the effectiveness of a sonar image but impacts viewers' general impression of a sonar image. These two factors are considered in the first stage: how much information will be extracted from images; and how comfortable the images are. The former can be measured by image entropy, since the variation of entropy introduced by distortion will disturb the extraction of useful information [28], while the latter is related to some high-order statistics. According to information theory [29], the entropy of an image is connected to the amount of information it contains. The entropy of a sonar image I is defined as

$$C_1 = H_I = -\sum_{i=0}^{255} P_i \log P_i \tag{1}$$

where i denotes the pixel value, P_i denotes the gray-level distribution of sonar image I.

According to some recent findings in neuroscience, the high-order statistics are related to human sense of "comfort." In this paper, the third- and fourth-order statistics (skewness and kurtosis) are adopted to reflect the comfort of perception. Skewness measures the asymmetry of probability distribution of a real-valued random variable about its mean. There exists a connection between skewed statistics and glossiness [30]. When a sonar image has a negative skewed statistics, it tends to appear lighter and less glossy than a similar image with higher skewness. We include the skewness defined as follows in the proposed PSIQP metric as the first comfort index:

$$C_2 = \text{skewness}(I) = E\left[\left(\frac{I - E(I)}{\sigma(I)}\right)^3\right] \tag{2}$$

where $\sigma(I)$ denotes the variance value of a sonar image I. In probability theory and statistics, kurtosis measures the "tailedness" of probability distribution of a real-valued random variable. Existing work shows that changes of absolute kurtosis value do occur when the perceptual comfort is reduced. The kurtosis employed as the second comfort index in this paper, and it is defined as

$$C_3 = \text{kurtosis}(I) = E\left[\left(\frac{I - E(I)}{\sigma(I)}\right)^4\right] - 3. \tag{3}$$

The information and comfort indices are extracted in the receiver side, and will be integrated into the proposed quality predictor alone with structural similarity to be introduced in the following section.

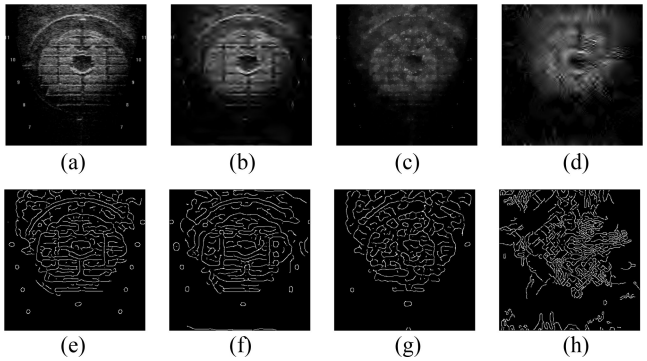

Fig. 3. Edge maps (bottom four images) extracted from sonar images (top four images). (a) Reference sonar image of a hull intake. (b) Sonar image distorted by SPIHT coding, MOS = 37.23. (c) Sonar image distorted by ComGBR coding, MOS = 34.07. (d) SPIHT-coded sonar image distorted by bit error, MOS = 26.84.

C. Structural Similarity

In the second stage, which related to image understanding, the structure becomes an important impacting factor of image quality since it is essential for object identification in most applications of sonar images. And the object identification is a reasonable approach to understand sonar images. The effectiveness of edge/gradient-based IQA methods along with their capability of representing image structure has been reported in [4], [31], and [32]. The edge map is employed in our PSIQP metric to represent the structural information of a sonar image. We illustrate its effect on object identification in Fig. 3. Fig. 3(a) shows the original sonar image of a hull intake, while Fig. 3(b)–(d) shows the distorted versions of Fig. 3(a). The mean opinion scores (MOSs), which represent the subjective opinions of image qualities, of distorted images are also provided in Fig. 3. As can be seen from Fig. 3(a)–(c), information is being lost as the decrease of image quality, but the contour (a representation of image structure) of main object still remain in the distorted images. According to the contour, we can approximately understand the image though many details have been lost due to distortion. When the structure has been totally destroyed, as shown in Fig. 3(d), we cannot understand the image since the object in it is hardly to be identified. The edge maps of these distorted images are shown in Fig. 3(e)–(h). We can conclude form Fig. 3(e)–(h) that edge maps can reflect the structure information for sonar images, which is important for image understanding. From the existing edge extractors, Canny operator is selected in the PSIQP metric for its good performance. The edge map extracted by Canny operator for a sonar image

is denoted by E. Then, considering the interplay between adjacent pixels, a median filter M is employed to reduce the impact of "blocking" artifacts [33]

$$E_M = E \otimes M_n \tag{4}$$

where n denotes that the size of the median filter is $n \times n$ and $\otimes$ denotes the convolution operation.

It is difficult to transmit E_M to the receiver side directly due to its big data volume, the information contained in E_M needs to be summarized with smaller amount of data. In terms of this issue, the normalized histogram is adapted to represent the distribution of E_M. Specially, the E_M is first preprocessed by being divided into $m \times m$ blocks considering the "uncrowded window." Research shows that the visual system recognizes an object by feature detection and combination. "Crowding" occurs when objects are too close together and features belong to several objects are combined into a jumbled percept. In most of the time, the human visual field is crowded, sparing only a central "uncrowded window." At a typical viewing distance, only the object in a local area within an "uncrowded window" can be distinguished clearly, and outside of this window, objects are too crowded to be distinguished. To identify objects that now lie outside of the window, we must move our eyes to bring our window to those objects [34]. Since we have considered the interplay between adjacent pixels by employing median filter in E, the blocks of edge map are nonoverlapping. Then, the normalized histogram $h(i)$ is established for edge map block E_M^i, where $i = 1, 2, \ldots, k$, k is the number of blocks for one edge map. The $h(i)$ is a two-dimensional array, two elements in which represent the probability of "edge" and "no edge" in this block respectively, since edge map is a binary image. The sum of these two elements is 1, so there is only one number need to be transmitted and compared for each edge map block. In this paper, the probability of "edge" is selected as the representation of normalized histogram for each block. The normalized histogram for edge map of the reference sonar image is denoted by $h_f(i)$, while the normalized histogram for edge map of the distorted sonar image is denoted by $h_d(i)$. Unlike E_M, $h_f(i)$, and $h_d(i)$ are not binary matrices. Finally, we measure the structural similarity $Q(i)$ for each block i by calculating the similarity of $h_f(i)$ and $h_d(i)$ using (5)

$$Q(i) = \frac{2h_f(i) \cdot h_d(i) + \delta}{h_f^2(i) + h_d^2(i) + \delta} \tag{5}$$

where δ is a small constant to avoid instability when $h_f^2(i) + h_d^2(i)$ is equal to 0.

In most cases, active areas are saliency areas, that is, objects in active areas attract more visual attention than objects in inactive areas. To take the influence of saliency into consideration, we assign the weight for $Q(i)$ according to the activity of corresponding image block. Since researchers analyze the received sonar image without reference information, only the activity of the received image will be considered in the proposed PSIQP metric. In receiver side, the received image is first divided into $m \times m$ blocks (the same size as the edge map block). The image activity measurement (IAM) [35] is then employed to detect the activity of each image block. The activity (IAM_0) of a $k_1 \times k_2$ image block b is defined as

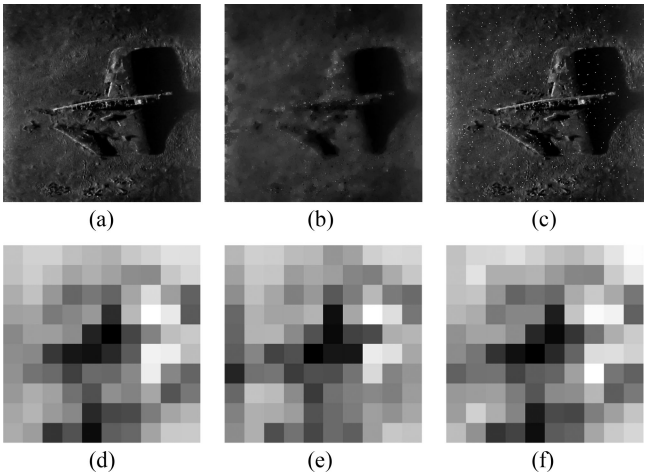

Fig. 4. Examples of the active maps of received sonar images. (a) Received sonar image with MOS = 69.32. (b) Received sonar image with MOS = 34.88. (c) Received sonar image with MOS = 55.74. Activity maps (bottom four images) of sonar images (top four images).

$$\mathrm{IAM}_0 = \frac{1}{k_1 \times k_2}[A' + B'] \tag{6}$$

where A' and B' are defined as

$$A' = \sum_{i=1}^{k_1-1} \sum_{j=1}^{k_2} |b(i, j) - b(i+1, j)|$$
$$B' = \sum_{i=1}^{k_1} \sum_{j=1}^{k_2-1} |b(i, j) - b(i, j+1)|. \tag{7}$$

The IAM is employed in each block of the received image to get the activity map $\mathrm{IAM}_{\mathrm{map}}$. The normalized activity map $\overline{\mathrm{IAM}}_{\mathrm{map}}$ is achieved as a weighting function of Q

$$\overline{\mathrm{IAM}}_{\mathrm{map}}(i) = \frac{\mathrm{IAM}_{\mathrm{map}}(i)}{\sum_{i=1}^{n} \mathrm{IAM}_{\mathrm{map}}(i)}. \tag{8}$$

Fig. 4 shows some examples of normalized activity maps for different received sonar images. For clearer observation, we enlarge the activity maps. As can be seen from Fig. 4, though top row images have different distortions, blocks that contain main object have higher activities. The weighted structural similarity for a received sonar image using the normalized activity map is obtained as

$$C_4 = \hat{Q} = \sum_{i=1}^{n} Q(i)\overline{\mathrm{IAM}}_{\mathrm{map}}(i). \tag{9}$$

D. Integration

We combine the information index, comfort indices, and structural similarity to generate the PSIQP metric

$$\mathrm{PSIQP} = \sum_{i=1}^{4} p_i \cdot C_i \tag{10}$$

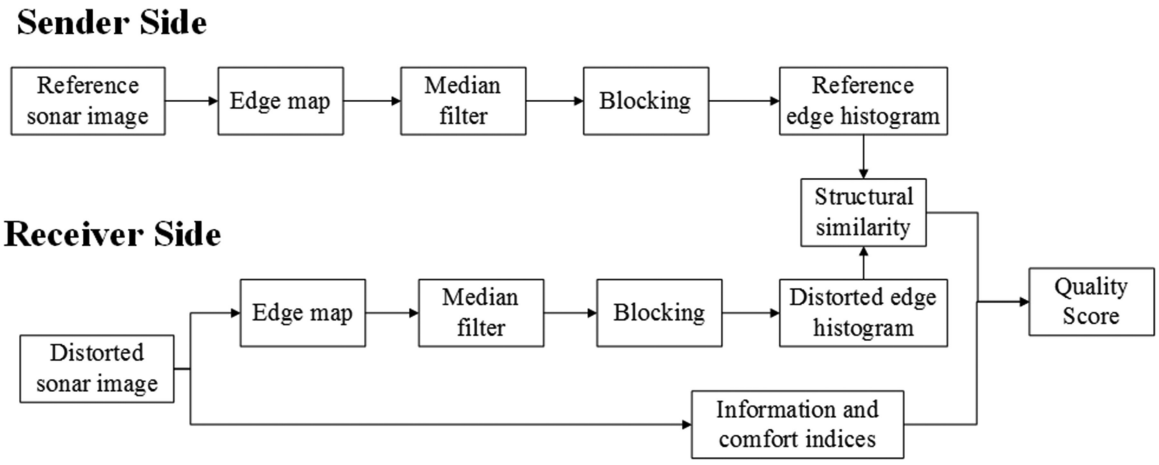

Fig. 5. Framework of the proposed PSIQP metric.

where p_1 to p_4 are weights of information index, comfort indices, and structural similarity. These parameters are determined as $p_1 = 0.169$, $p_2 = -1.614$, $p_3 = 0.196$, $p_3 = 54.46$. The determination of these parameters will be analyzed in following section. The framework of the proposed PSIQP metric is shown in Fig. 5.

III. EXPERIMENTAL RESULTS AND ANALYSIS

A. Database and Evaluation Protocols

The performance of the proposed PSIQP metric is validated in the SIQD database [36], which consists of images captured by acoustic lens sonar or side-scan sonar. The SIQD database contains 40 reference images with some typical underwater scenes, such as swimmer, underwater creatures, seabed, and shipwrecks. As presented in Fig. 6, these reference images are corrupted by compression and bit errors to generate distorted images with four distortion types at four to six distortion levels. Two types of compressed sonar images in the SIQD database are obtained using ComGBR coding [37] and SPIHT coding [38], which provide with good robustness and high compressibility, respectively. The other two types of distorted images due to bit error are collected by making man-made bit error in bitstreams after SPIHT coding and ComGBR coding, respectively. Each image in the SIQD database is subjectively rated by at least 25 viewers, then the MOS for each image is collected. For more details about the subjective experiments to collect MOSs, readers can refer to [36]. Overall, the SIQD database gathered 40 reference images and 800 distorted images along with their MOSs to be used in this study.

A logistic procedure is applied in this paper between MOSs s_m and objective scores s_o to remove the nonlinearity caused by subjective rating process

$$s_p = \beta_1 \left(\frac{1}{2} - \frac{1}{1 + \exp\left(\beta_2 (s_o - \beta_3)\right)} \right) + \beta_4 s_o + \beta_5 \quad (11)$$

where s_p denotes IQA score after regression, and β_1 to β_5 are parameters of the regression model. To prevent correlation value from being lowered too much by a misordering of human performance values that are nearly identical [39], an isotonic (or monotonic) regression is employed between s_m and s_o

$$s_{\text{mono}} = f \uparrow \bigcup f \downarrow \quad (12)$$

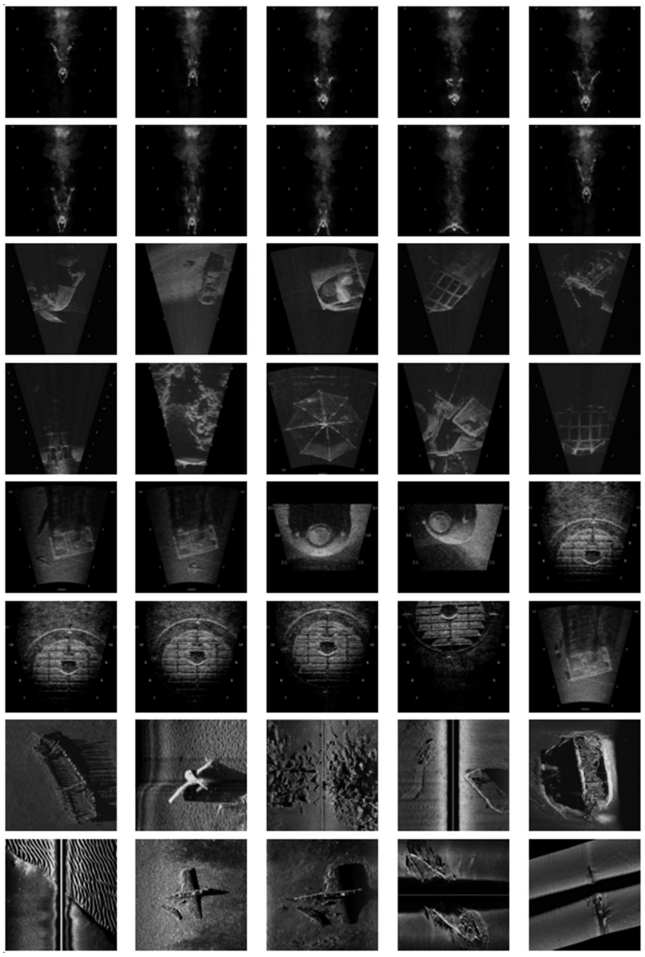

Fig. 6. Reference sonar images.

TABLE I
Performance Comparisons Among RR IQA Models on the SIQD Database

Class	Criteria	QMC	RWQMS	OSVP	SDM	RIQMC	PSIQP
1	θ_s	**0.723**	0.563	0.670	0.519	0.434	0.665
	θ_k	**0.532**	0.396	0.480	0.355	0.300	0.476
	θ_p	**0.783**	0.599	0.703	0.539	0.608	0.673
	θ_r	**8.027**	10.328	9.165	10.864	10.237	9.543
	θ_m	**6.436**	8.094	7.225	8.408	8.175	7.772
2	θ_s	0.562	0.249	0.664	0.596	0.491	**0.674**
	θ_k	0.393	0.161	0.464	0.405	0.346	**0.482**
	θ_p	0.582	0.477	0.680	0.634	0.538	**0.683**
	θ_r	9.234	9.986	8.328	8.780	9.573	**8.295**
	θ_m	7.305	7.972	6.748	7.185	7.507	**6.469**
3	θ_s	0.318	0.721	**0.807**	0.618	0.377	0.757
	θ_k	0.287	0.504	**0.632**	0.433	0.302	0.572
	θ_p	0.633	0.783	**0.819**	0.643	0.652	0.763
	θ_r	12.099	9.720	**8.974**	10.710	11.851	10.115
	θ_m	9.226	7.257	**6.218**	8.445	9.317	7.280
4	θ_s	0.631	0.669	0.598	0.652	0.394	**0.847**
	θ_k	0.438	0.490	0.415	0.460	0.278	**0.649**
	θ_p	0.656	0.718	0.603	0.637	0.552	**0.850**
	θ_r	10.431	9.624	11.032	10.659	11.531	**7.287**
	θ_m	8.462	7.767	9.070	8.723	9.447	**5.665**
Overall	θ_s	0.468	0.542	0.618	0.706	0.361	**0.759**
	θ_k	0.328	0.383	0.433	0.512	0.248	**0.565**
	θ_p	0.585	0.582	0.643	0.717	0.546	**0.764**
	θ_r	11.344	11.374	10.710	9.751	11.715	**9.022**
	θ_m	8.957	8.911	8.445	7.652	9.430	**7.041**

where $f \uparrow = h(\cdot) : h(w) \geq h(z), \forall w > z$ and $f \downarrow = h(\cdot) : h(w) \leq h(z), \forall w > z, w, z \in s_o$. We estimate the performance of an IQA metric from the following three aspects in this paper.

1) Prediction monotonicity, which is measured by Spearman rank order correlation coefficient (θ_s) and Kendall's rank order correlation coefficient (θ_k) between s_m and s_o.
2) Prediction accuracy that is judged by Pearson linear correlation coefficient (θ_p) between s_m and s_p.
3) Prediction consistency, which can be estimated using root mean square (θ_r), mean absolute error (θ_m) between s_m and s_p, and monotonic correlation coefficient (θ_{mono}) between s_m and s_{mono}.

High values in θ_s, θ_k, θ_p, and θ_{mono}, and low values in θ_r and θ_m mean superior correlation with subjective scores.

To evaluate the performance of proposed PSIQP metric, we compare it with five RR IQA metrics and eleven FR IQA metrics. The selected IQA metrics for performance comparison include:

1) classical FR PSNR, SSIM [33], VSNR [40];
2) state-of-the-art FR FSIM [41], MAD [42], VSI [43], GMSD [31], PSIM [32], GSM [4], ADD-SSIM [44], LTG [45];
3) popular RR OSVP [13], RIQMC [14], SDM [15], QMC [12], RWQMS [16].

They all have achieved good performances for NSIs.

TABLE II
Comparison of the Statistical Significances of the PSIQP Metric and Five RR IQA Metrics on the SIQD Database

Metrics	QMC	RWQMS	SDM	OSVP	RIQMC
Index	$+1$	$+1$	$+1$	$+0$	$+1$

TABLE III
Comparison of θ_{mono} of the PSIQP Metric and Five RR IQA Metrics on the SIQD Database

Metrics	QMC	RWQMS	SDM	OSVP	RIQMC	PSIQP
θ_{mono}	0.581	0.624	0.674	0.740	0.532	**0.778**

B. Performance Measures and Statistical Significance

Performance comparisons between proposed PSIQP and five RR IQA metrics are tabulated in Table I. We highlight the best-performing algorithm in bold font, and the second-performing algorithm by underline. To test the performances of IQA metrics for different distortions belonging to the SIQD database, we group test images by distortion types such that images distorted by ComGBR compression coding and SPIHT compression coding as "Class 1" and "Class 2," respectively, those distorted by bit error in ComGBR and SPIHT bitstreams as "Class 3" and "Class 4," respectively. Sonar images in "Class 1" are mainly corrupted by a kind of blur caused by ComGBR, which is a compression coding scheme based on compressed sensing, while noneccentricity distortion and another blur-like distortion caused by SPIHT is main distortion contained in sonar images of "Class 2." Sonar images in "Class 3" mainly contain noise. There are messy, unnatural marks in sonar images from "Class 4."

As listed in Table I, the proposed PSIQP metric is among the best for most of distortions in the SIQD database. For "Class 2" and "Class 4," our PSIQP metric has gained the best prediction accuracy, monotonicity, and consistency. To specify, for "Class 4," the PSIQP metric acquires the prediction monotonicity (θ_s) of beyond 0.84, the prediction accuracy (θ_p) of larger than 0.85. Almost all the selected RR IQA metrics fail on images from "Class 2" though the proposed model shows the best performance among them, which indicates that the noneccentricity distortion may confuse the prediction of subjective quality. For "Class 3," the PSIQP metric is among the best in the comparison of prediction monotonicity (θ_s and θ_k). For prediction accuracy and consistency, our metric is a little worse than RWQMS and OSVP. And among selected testing RR IQA metrics, only these three IQA metrics (RWQMS, OSVP, and PSIQP) show reasonable performance for "Class 3." For "Class 1." the QMC and OSVP are matchable with (in fact, a little inferior than) our metric. Among these four distortion types included in the SIQD database, the worst prediction monotonicity (θ_s) gained by the PSIQP metric is 0.665, the worst prediction accuracy (θ_p) is 0.673, the worst prediction consistency (θ_r) is 9.543, while the other selected RR IQA metrics may achieve good performance at one distortion

TABLE IV
Performance Comparisons Between Eleven FR IQA Metrics and Proposed PSIQP Metric Based on the SIQD Database

Criteria	SSIM	PSNR	VSNR	FSIM	VSI	GMSD	ADD-SSIM	MAD	GSM	PSIM	LTG	PSIQP
θ_s	0.654	0.622	0.433	0.706	0.720	0.724	0.723	0.717	0.642	0.727	0.675	**0.759**
θ_k	0.469	0.443	0.299	0.510	0.523	0.521	0.524	0.526	0.455	0.528	0.481	**0.565**
θ_p	0.673	0.639	0.476	0.721	0.736	0.730	0.742	0.736	0.658	0.738	0.684	**0.764**
θ_r	10.345	10.760	11.980	9.687	9.219	9.554	9.376	9.471	10.533	9.433	10.195	**9.022**
θ_m	8.066	8.540	9.772	7.589	7.148	7.646	7.397	7.393	8.289	7.492	8.103	**7.041**

TABLE V
Complexity Comparison (Seconds/Image) of the PSIQP Metric and Four RR IQA Metrics on the SIQD Database

Metrics	QMC	RWQMS	SDM
Cost (s)	2.92×10^{-2}	4.04×10^{-1}	5.13×10^{-1}
Metrics	OSVP	RIQMC	PSIQP
Cost (s)	5.10×10^{-2}	1.41	1.69×10^{-1}

type but behave badly at the other distortion types. This indicates that the robustness of the PSIQP metric across four distortion types contained in the SIQD database is better than other selected RR IQA metrics'. To conduct an overall comparison on the entire SIQD database, we tabulate the performances of all the selected RR IQA metrics and the proposed PSIQP metric in the last five rows of Table I. It is obvious that the proposed PSIQP beats other competing quality measures. Only the PSIQP metric achieves performances greater than 0.75 for θ_s and θ_p and greater than 0.56 for θ_k, but lower than 9.1 for θ_r and lower than 7.1 for θ_m. Relative to the second-ranking RR IQA metric, the performance gain of the proposed PSIQP metric is around 7.5% in terms of θ_s, 10% in terms of θ_k and over 6.5%, 7%, 7.9% in terms of θ_p, θ_r, and θ_m, respectively, which indicates the promotion in performance accuracy, consistency, and monotonicity.

The comparison of statistical significance is conducted in this paper by calculating residuals of the PSIQP metric and each of selected RR IQA metrics using F-test with assumption that the significance level is 0.05. As tabulated in Table II, symbols "+1," "0," and "−1" mean that the proposed PSIQP metric performs statistically (with 95% confidence) better, undistinguishable and worse than corresponding test RR metric, respectively. The results show that the PSIQP metric is statistically better than most of the selected RR IQA metrics (QMC, RWQMS, SDM, RIQMC), and equivalent to the OSVP.

Since not all the possible monotonic functions can be captured by the logistic function, which is used in θ_p, θ_{mono} provides a reasonable measurement of how well a monotonic function fits the sequence pair by employing an isotonic regression. Table III shows θ_{mono} of the PSIQP metric and five RR IQA metrics on the SIQD database. Obviously, the proposed PSIQM shows the highest θ_{mono}, which indicates that it is a worthier quality measure when compared with selected RR IQA metrics for sonar images on the SIQD database [39].

We also include the performance comparison results of the proposed PSIQP metric with eleven FR IQA metrics as shown in Table IV. The results validate the superiority of the proposed PSIQP metric on the SIQD database, beating other selected FR quality models. The other conclusions that can be obtained from Table IV are as follows.

1) The state-of-the-art FR IQA metrics show worse performances than our PSIQP metric but perform better than classical IQA metrics on the SIQD database.
2) Except our PSIQP metric, the PSIM shows the best prediction monotonicity.
3) The ADD-SSIM achieves the second best prediction accuracy while the best one is the PSIQP metric.
4) The prediction consistency acquired by VSI is only worse than the proposed PSIQP metric but better than the rest of the FR IQA metrics.

C. Testing of the Parameter Sensitivity

Since the contents included by a database are limited, the performance of quality model may be influenced by the contents of the test images to some extent. A good IQA method must be content-insensitive, while a poor IQA method is very dependent on the training set. We test the sensitivity of four parameters used in the integration stage as shown in (10). The values of these four parameters are determined after 100 parameter fitting processes with different content grouping. The SIQD database is divided into one training set with 672 images of 32 kinds of contents and one test set, which includes 168 images of the other eight kinds of contents in each process. The above division is repeated 100 times, the parameter fitting process is run over 100 iterations, and 100 groups of weighting parameters are obtained as shown in Fig. 7. The dots indicate 100 fitting results, while the five-pointed star, asterisks, horizontal line in the box, bottom and top of the box indicate the mean value, the maximum and minimum value, median value, upper and lower quartile of these 100 fitting results, respectively. It is obvious that weighting parameters obtained from 100 parameter fitting processes are different but distribute in a small range, which indicates the insensitivity of weighting

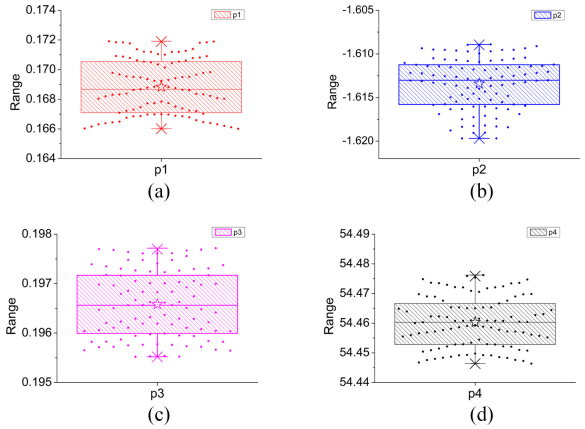

Fig. 7. Results distributions and box plots of 100 fitting processes. (The horizontal axes corresponds to the weighting parameters, and the vertical axes corresponds to the fitting results of four parameters.)

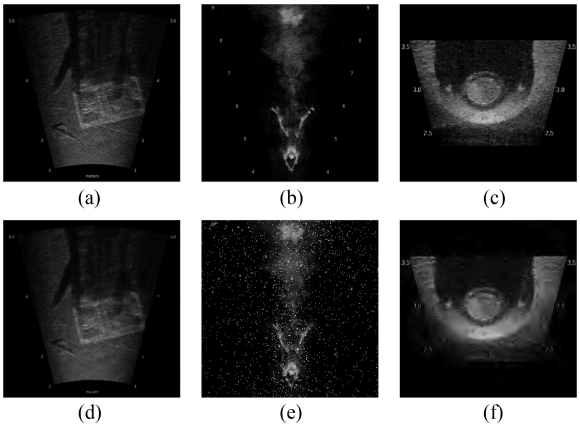

Fig. 8. Examples of the quality predictions provided by the PSIQM metric. (a)–(c) Reference SIs. (d) Distorted version of (a), MOS = 54.23, PSIQM score = 54.19. (e) Distorted version of (b), MOS = 29.79, PSIQM score = 30.01. (f) Distorted version of (c), MOS = 49.19, PSIQM score = 49.26.

parameters. Then, we determine the weighting parameters using mean values of fitting results of 100 iterations.

D. Complexity Comparison

The average consuming times of the proposed PSIQP metric and four selected RR IQA metrics on the overall 840 images of size 320×320 in the SIQD database are tabulated in Table V. The comparison of computational costs were run using the software platform of MATLAB R2012b on a computer with 3.20 GHz CPU processor and 8.00 GB RAM. We obtain the source codes of selected RR IQA metrics from their authors or websites. It can be observed in Table V that our PSIQP metric is about three times faster than the SDM, which performs second only to the PSIQP metric.

E. Intuitive Comparison

For visual comparison, Fig. 8 shows examples of the quality predictions provided by the PSIQM metric, which are very close to the actual human performance (MOS values) provided by the SIQD database. The scatter plots between MOS and quality predictions yielded by five selected RR IQA metrics and the PSIQP metric are presented in Fig. 9. In each scatter plot, distinct symbols are used to discriminate different distortion types as mentioned in Section III-B: Red circle for "Class 1," green square for "Class 2," deep-blue diamonds for "Class 3," blue triangle for "Class 4," and purple inverted triangle for reference images without any distortion. Compared with the scatter plots of the other RR IQA metrics, qualities predicted by our PSIQP metric show the best correlation to MOSs. And for different distortion classes, the proposed PSIQP metric is robust across four types of distortions contained in the SIQD database though there are still some aberrant data points. As shown in Fig. 9, most aberrant data points are from "Class 3," that is, the sample points associated with "Class 3" are away from the sample points belong to the other three distortion types. These aberrant points are the optimization objects for further work.

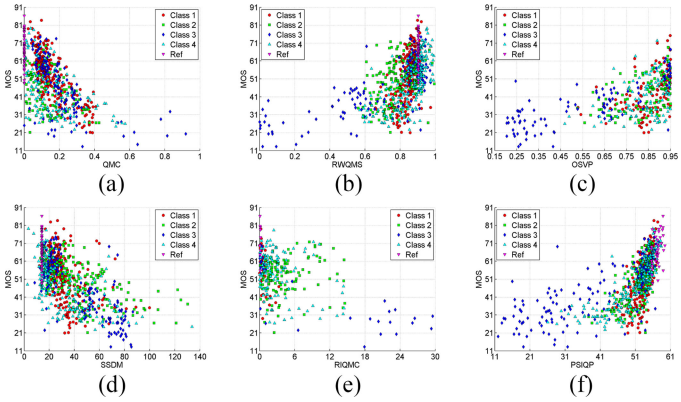

Fig. 9. Scatter plots of MOS versus model predictions. Each sample point stands for a test image. (a) QMC. (b) RWQMS. (c) OSVP. (d) SDM. (e) RIQMC. (f) PSIQP.

F. Discussion and Future Work

Actually, there is another issue about RR IQA deserving further discussion and research, that is, the transmission scheme of reference signal. A reliable transmission scheme of reference signal is crucial for RR IQA metric, since the comparison between reference and distorted signal has great influence on the predicted quality. Many relative researches, such as [16], [46], tend to assume an ancillary channel that is error-free. In this situation, to tackle the problem, the following operations may make the differences:

1) compressing the data volume of reference signal;
2) increasing the code redundancy for more powerful error-correcting ability;
3) reducing the data rate.

Since the UAC only provides with relatively limited bandwidth and unstable link, for such ancillary UAC, the reliability needs further discussion and experiments.

Apart from the ancillary channel, another possible solution is to embed the reference signal in the transmitted image as a watermark. To accomplish the task of carry-

ing reference signal without distortion (or with acceptable distortions) to the receiver, the watermark should have following features. The first is the invisibility, that is, the embedding of watermark should not influence the quality of the carrier image. The second is the robustness to ensure reliable transmission of reference signal. Since the reference signal represents the information of original images, the damage of it will lead to quality evaluation error. The last one is blind extraction to ensure reliable receiving of reference signal. Nowadays, there are many research results concerning invisible watermark achieving reasonable robustness and blind extraction [47]–[51]. Despite the problems such as the robustness is kind of dependent on the content of carrier images and limited embedding capacity, watermark shows its potential of being reliable carrier of reference signal, and some further efforts can be made to enhance the performance of watermark.

IV. CONCLUSION

Sonar images are important for ocean engineering since they very possibly contain important information such as submarine geomorphology, marine organism, wreck remains, and so on. The differences between sonar images and NSIs, SCIs, stereoscopic images, and medical images, etc., in imaging mechanism, image characteristics, and utilities lead to the failure of existing IQA methods on evaluation of sonar image quality. Since one of the most complicated channels should be the UAC, and the reference signal is not entirely available for underwater transmission, we establish a RR sonar IQA metric (PSIQP) based on the consideration of both image perception and image understanding in this paper. Results of experiments present that, in comparison to the relevant state-of-the-art RR and FR IQA models on SIQD database that consists of 840 sonar images (40 reference sonar images and 800 sonar images distorted in the process of underwater transmission simulation), the PSIQP metric shows better performance. The source code of new model will be released to the public. In future work, the transmission of reference signal will be discussed, and the watermark will be considered to achieve reliable transmission of reference signal in underwater condition.

REFERENCES

[1] D. Clark, I. Ruiz, Y. Petillot, and J. Bell
Particle PHD filter multiple target tracking in sonar image
IEEE Trans. Aerosp. Electron. Syst., vol. 43, no. 1, pp. 409–416, Jan. 2007.

[2] K. Lo and B. Ferguson
Automatic detection and tracking of a small surface watercraft in shallow water using a high-frequency active sonar
IEEE Trans. Aerosp. Electron. Syst., vol. 40, no. 4, pp. 1377–1388, Oct. 2004.

[3] K. Gu, D. Tao, J.-F. Qiao, and W. Lin
Learning a no-reference quality assessment model of enhanced images with big data
IEEE Trans. Neural Netw. Learn. Syst., vol. 29, no. 4, pp. 1301–1313, Apr. 2018.

[4] A. Liu, W. Lin, and M. Narwaria
Image quality assessment based on gradient similarity
IEEE Trans. Image Process., vol. 21, no. 4, pp. 1500–1512, Apr. 2012.

[5] K. Gu, G. Zhai, X. Yang, L. Chen, and W. Zhang
Nonlinear additive model based saliency map weighting strategy for image quality assessment
In *Proc. IEEE Int. Workshop Multimedia Signal Process.*, Sep. 2012, pp. 313–318.

[6] K. Gu, J. Zhou, J.-F. Qiao, G. Zhai, W. Lin, and A. C. Bovik
No-reference quality assessment of screen content pictures
IEEE Trans. Image Process., vol. 26, no. 8, pp. 4005–4018, Aug. 2017.

[7] K. Gu, G. Zhai, X. Yang, and W. Zhang
Using free energy principle for blind image quality assessment
IEEE Trans. Multimedia, vol. 17, no. 1, pp. 50–63, Jan. 2015.

[8] F. Shao, W. Lin, S. Wang, G. Jiang, M. Yu, and Q. Dai
Learning receptive fields and quality lookups for blind quality assessment of stereoscopic images
IEEE Trans. Cybern., vol. 46, no. 3, pp. 730–743, Mar. 2015.

[9] F. Shao, W. Lin, S. Wang, G. Jiang, and M. Yu
Blind image quality assessment for stereoscopic images using binocular guided quality lookup and visual codebook
IEEE Trans. Broadcast., vol. 61, no. 2, pp. 154–165, Jun. 2015.

[10] S. Li and R. Paramesran
Review of medical image quality assessment
Biomed. Signal Process. Control, vol. 27, pp. 145–154, May 2016.

[11] K. Gu, S. Wang, H. Yang, W. Lin, G. Zhai, X. Yang, and W. Zhang
Saliency-guided quality assessment of screen content images
IEEE Trans. Multimedia, vol. 18, no. 6, pp. 1–13, Jun. 2016.

[12] K. Gu, G. Zhai, X. Yang, W. Zhang, and C. W. Chen
Automatic contrast enhancement technology with saliency preservation
IEEE Trans. Circuits Syst. Video Technol., vol. 25, no. 9, pp. 1480–1494, Sep. 2015.

[13] J. Wu, W. Lin, G. Shi, L. Li, and Y. Fang
Orientation selectivity based visual pattern for reduced-reference image quality assessment
Inf. Sci., vol. 351, pp. 18–29, Mar. 2016.

[14] K. Gu, G. Zhai, W. Lin, and M. Liu
The analysis of image contrast: From quality assessment to automatic enhancement
IEEE Trans. Cybern., vol. 46, no. 1, pp. 284–297, Jan. 2016.

[15] K. Gu, G. Zhai, X. Yang, and W. Zhang
A new reduced-reference image quality assessment using structural degradation model
In *Proc. IEEE Int. Symp. Circuits Syst.*, May 2013, pp. 1095–1098.

[16] S. Wang, K. Gu, X. Zhang, W. Lin, L. Zhang, S. Ma, and W. Gao
Subjective and objective quality assessment of compressed screen content images
IEEE J. Emerg. Sel. T. Circuits Syst., vol. 6, no. 4, pp. 532–543, Dec. 2016.

[17] T. Liu, Y. Lin, W. Lin, and C. Kuo
Visual quality assessment: Recent developments, coding applications and future trends
Apsipa Trans. Signal Inf. Process., vol. 2, pp. 1–20, 2013.

[18] D. Rouse, S. Hemami, R. Pepion, and L. Patrick
Estimating the usefulness of distorted natural images using an image contour degradation measure
J. Opt. Soc. Amer. A, Opt., Image Sci. Vis., vol. 28, no. 2, pp. 157–188, 2011.

[19] D. Rouse, R. Pepion, S. Hemami, and P. Callet
Image utility assessment and a relationship with image quality assessment
In Proc. SPIE, vol. 7240, 2009, Art. no. 724010.

[20] D. Rouse, R. Pepion, P. Callet, and S. Hemami
Tradeoffs in subjective testing methods for image and video quality assessment
Hum. Vis. Electron. Imaging XV, vol. 7527, 2010, Art. no. 75270F.

[21] M. Stojanovic and L. Freitag
Recent trends in underwater acoustic communications
Marine Technol. Soc. J., vol. 47, no. 5, pp. 45–50, Sep. 2013.

[22] X. Yu, Y. Li, W. Yang, and Y. Sun
Design and analysis of unequal error protection rateless spinal codes
IEEE Trans. Commun., vol. 64, no. 11, pp. 4461–4473, Nov. 2016.

[23] J. Wu, G. Shi, W. Lin, A. Liu, and F. Qi
Just noticeable difference estimation for images with free-energy principle
IEEE Trans. Multimedia, vol. 15, no. 7, pp. 1705–1710, Nov. 2013.

[24] A. Webster, C. Jones, M. Pinson, D. Voran, and S. Wolf
An objective video quality assessment system based on human perception
In *Proc. SPIE*, vol. 1913, 1993, pp. 1–12.

[25] C. Hewage and M. Martini
Edge-based reduced-reference quality metric for 3-D video compression and transmission
IEEE J. Sel. Topics Signal Process., vol. 6, no. 5, pp. 471–482, Sep. 2012.

[26] A. Abdul and M. Isa
Underwater image quality enhancement through composition of dual-intensity images and Rayleigh-stretching
Springerplus, vol. 3, no. 1, pp. 218–219, Sep. 2014.

[27] H. Lu, Y. Li, X. Xu, D. Donaled, and S. Seiichi
Underwater image descattering and quality assessment
In *Proc. IEEE Int. Conf. Image Process.*, Sep. 2016, pp. 1998–2002.

[28] J. Kalwa and A. Madsen
Sonar image quality assessment for an autonomous underwater vehicle
In *Proc. World Autom. Congress*, 2004, pp. 33–38.

[29] C. Shannon
A mathematical theory of communication
Bell Syst. Tech. J., vol. 27, no. 3, pp. 379–423, Oct. 1948.

[30] I. Motoyoshi, S. Nishida, L. Sharan, and E. Adelson
Image statistics and the perception of surface qualities
Nature, vol. 447, no. 7141, pp. 206–209, May 2007.

[31] W. Xue, L. Zhang, X. Mou, and A. Bovik
Gradient magnitude similarity deviation: A highly efficient perceptual image quality index
IEEE Trans. Image Process., vol. 23, no. 2, pp. 684–695, Feb. 2014.

[32] K. Gu, L. Li, H. Lu, X. Min, and W. Lin
A fast reliable image quality predictor by fusing micro- and macro-structures
IEEE Trans. Ind. Electron., vol. 64, no. 5, pp. 3903–3912, May 2017.

[33] Z. Wang, A. Bovik, H. Sheikh, and E. Simoncelli
Image quality assessment: From error visibility to structural similarity
IEEE Trans. Image Process., vol. 13, no. 4, pp. 600–612, Apr. 2004.

[34] D. Pelli and K. Tillman
The uncrowded window of object recognition
Nature Neurosci., vol. 11, no. 10, pp. 1129–1135, Oct. 2008.

[35] S. Saha and R. Vemuri
An analysis on the effect of image activity on lossy coding performance
In *Proc. IEEE Int. Symp. Circuits Syst.*, 2000, vol. 3, pp. 295–298.

[36] W. Chen, F. Yuan, E. Cheng, and W. Lin
Subjective and objective quality evaluation of sonar images for underwater acoustic transmission
In *Proc. Int. Conf. Image Process.*, 2017, pp. 176–180.

[37] W. Chen, F. Yuan, and E. Cheng
Adaptive underwater image compression with high robust based on compressed sensing
In *Proc. IEEE Int. Conf. Signal Process., Commun. Comput.*, 2016, pp. 1–6.

[38] A. Said and W. Pearlman
A new, fast, and efficient image codec based on set partitioning in hierarchical trees
IEEE Trans. Circuits Syst. Video Technol., vol. 6, no. 3, pp. 243–250, Jun. 1996.

[39] L. Kaplan, D. Stephen, S. Rick, and K. Richard
Analysis of image quality for image fusion via monotonic correlation
IEEE J. Sel. Topics Signal Process., vol. 3, no. 2, pp. 222–235, Apr. 2009.

[40] D. Chandler and S. Hemami
VSNR: A wavelet-based visual signal-to-noise ratio for natural images
IEEE Trans. Image Process., vol. 16, no. 9, pp. 2284–2298, Sep. 2007.

[41] L. Zhang, L. Zhang, X. Mou, and D. Zhang
FSIM: A feature similarity index for image quality assessment
IEEE Trans. Image Process. A Pub. IEEE Signal Process. Soc., vol. 13, no. 8, pp. 2378–2386, Aug. 2011.

[42] E. Larson and D. Chandler
Most apparent distortion: Full-reference image quality assessment and the role of strategy
J. Electron. Imag., vol. 19, no. 1, pp. 1–6, Jan. 2010.

[43] L. Zhang, Y. Shen, and H. Li
VSI: A visual saliency-induced index for perceptual image quality assessment
IEEE Trans. Image Process., vol. 23, no. 10, pp. 4270–4281, Oct. 2014.

[44] K. Gu, S. Wang, G. Zhai, W. Lin, X. Yang, and W. Zhang
Analysis of distortion distribution for pooling in image quality prediction
IEEE Trans. Broadcast., vol. 62, no. 2, pp. 446–456, Jun. 2016.

[45] K. Gu, G. Zhai, X. Yang, and W. Zhang
An efficient color image quality metric with local-tuned-global model
In *Proc. IEEE Int. Conf. Image Process.*, Oct. 2014, pp. 506–510.

[46] A. Radosevic, R. Ahmed, T. Duman, G. Proakis, and M. Stojanovic
Adaptive OFDM modulation for underwater acoustic communications: Design considerations and experimental results
IEEE J. Ocean. Eng., vol. 39, no. 2, pp. 357–370, Apr. 2014.

[47] P. Kulkarni, A. Mulani, and P. Mane
Robust invisible watermarking for image authentication
In *Proc. Int. Conf. Emerg. Trends Electr., Commun. Inf. Technol.*, Dec. 2017, pp. 193–200.

[48] B. Jagadeesh, P. Kumar, and P. Reddy
Robust digital image watermarking based on fuzzy inference system and back propagation neural networks using DCT
Soft Comput., vol. 20, no. 9, pp. 1–8, Sep. 2016.

[49] H. Bi, X. Li, Y. Zhang, and Y. Xu
A robust CT-SVD composite watermarking scheme
J. Comput. Inf. Syst., vol. 6, no. 3, pp. 873–880, Mar. 2010.

[50] D. Coltuc
Towards distortion-free robust image authentication
J. Phys., Conf., vol. 77, no. 1, p. 12005, 2007.

[51] Y. Zhang, H. Bi, and H. Zhang
Robust watermarking scheme by harris interest regions
J. Comput. Inf. Syst., vol. 8, no. 20, pp. 8421–8429, Oct. 2012.

Weiling Chen received the B.S. degree in communication engineering from Xiamen University, Xiamen, China, in 2013. She is currently working toward the Ph.D. degree in communication and information system at Xiamen University, Xiamen, China.

From September 2016 to December 2016, she was a visiting scholar at the School of Computer Science and Engineering, Nanyang Technological University, Singapore. Her current research interests include image quality assessment, image compression, and underwater acoustic communication.

Ms. Chen is the Reviewer for IEEE International Conference on Image Processing (ICIP) in 2016, ICIP 2017, IEEE ACCESS, and T-IP.

Ke Gu received the B.S. and Ph.D. degrees in electronic engineering from Shanghai Jiao Tong University, Shanghai, China, in 2009 and 2015, respectively.

His research interests include image quality assessment and air quality prediciton. Dr. Gu is the Associated Editor for IEEE ACCESS and Reviewer for 20 top SCI journals. He was the recipient of the Best Paper Award for the IEEE International Conference on Multimedia and Expo and Excellent Ph.D. thesis award from the Chinese Institute of Electronics in the year of 2016. He is the leading organizer of special session in VCIP2016 and ICIP2017.

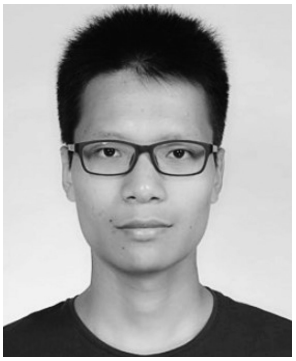

Xiongkuo Min received the B.E. degree in electronics and information engineering from Wuhan University, Wuhan, China, in 2013. He is currently working toward the Ph.D. degree in information and communication engineering with the Institute of Image Communication and Network Engineering, Shanghai Jiao Tong University, Shanghai, China.

From 2016 to 2017, he was a visiting student with the Department of Electrical and Computer Engineering, University of Waterloo, Waterloo, ON, Canada. His research interests include image quality assessment, visual attention modeling, and perceptual signal processing.

Mr. Min received the Best Student Paper Award of International Conference on Multimedia and Expo 2016.

Fei Yuan received the B.S., M.S., and Ph.D. degrees in electronic engineering from Xiamen University, Xiamen, China, in 2002, 2005, and 2008, respectively.

He is currently an Associate Professor and a Supervisor for master with Xiamen University. His main research interests include underwater acoustic communication, marine information, image processing, and embedded system.

Dr. Yuan is the member of China Institute of Communications, the Acoustical Society of China, and IET. He is the reviewer for Journal of Xiamen University, Chinese Journal of Acoustics, Chinese Journal of Scientific Instrument, Applied Acoustic, IJNAOE, etc. He is also the review of provincial and state projects such as Natural Science Foundation of China, scientific planning subjects of Xiamen, etc.

En Cheng received the B.S., M.S., and Ph.D. degrees in electronic engineering from Xiamen University, Xiamen, China, in 1985, 1988, and 2006, respectively.

He is currently a Professor and a Supervisor for Ph.D. candidates with Xiamen University. He is the standing Deputy Director with the Key Laboratory of Underwater Acoustic Communication and Marine Information Technology, Ministry of Education, Xiamen University. Since 2002, he has been the senior member of the Chinese Institute of Electronics. From 2003 to 2012, he was the Department Head with the Department of Communication Engineering, Xiamen University. He authored and coauthored more than 50 papers in international journals and conferences. His main research interests include underwater acoustic communication and networks.

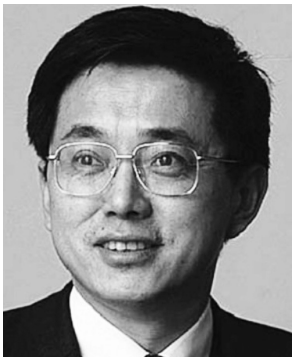

Wenjun Zhang (F'11) received the B.S., M.S., and Ph.D. degrees in electronic engineering from Shanghai Jiao Tong University, Shanghai, China, in 1984, 1987, and 1989, respectively.

From 1990 to 1993, He was a Postdoctoral Fellow with Philips Kommunikation Industrie AG, Nuremberg, Germany, where he was actively involved in the developing HD-MAC system. He was the Faculty of Shanghai Jiao Tong University, Shanghai, China, in 1993 and became a Full Professor with the Department of Electronic Engineering in 1995. As the national HDTV TEEG project leader, he successfully developed the first Chinese HDTV prototype system in 1998. He was one of the main contributors to the Chinese Digital Television Terrestrial Broadcasting Standard issued in 2006 and is leading team in designing the next generation of broadcast television system in China from 2011. He holds more than 40 patents and authored or coauthored more than 90 papers in international journals and conferences. His main research interests include digital video coding and transmission, multimedia semantic processing, and intelligent video surveillance. He is a Chief Scientist of the Chinese National Engineering Research Centre of Digital Television, an industry/government consortium in DTV technology research and standardization, and the Chair of Future of Broadcast Television Initiative Technical Committee.